CHEMISTRY OF MATERIALS

pubs.acs.org/cm

Article

# Mechanism of Thermal Atomic Layer Etching of Hafnium Zirconium Oxide, $HfO_2$ and $ZrO_2$ Using Sequential HF and Acetylacetone Exposures

Troy A. Colleran, Aziz I. Abdulagatov, Jonathan L. Partridge, Andrew S. Cavanagh, and Steven M. George*

Cite This: *Chem. Mater.* 2025, 37, 5935−5945

Read Online

ACCESS | Metrics & More | Article Recommendations



**ABSTRACT:** The mechanism of hafnium zirconium oxide (HZO), $HfO_2$ and $ZrO_2$ thermal atomic layer etching (ALE) was explored using sequential hydrogen fluoride (HF) and acetylacetone (Hacac) exposures. HF modifies the metal oxide surface by forming a metal fluoride layer. Hacac then removes the metal fluoride layer by forming volatile metal acac products. Initial in situ spectroscopic ellipsometry investigations revealed that amorphous and crystalline HZO, $HfO_2$ and $ZrO_2$ films were etched by sequential HF and Hacac exposures. Amorphous HZO was etched at a rate of 0.80 Å/cycle at 230 °C. Crystalline HZO was etched at rates of 0.50 and 0.74 Å/cycle at 250 and 270 °C, respectively. Amorphous $HfO_2$ and $ZrO_2$ were etched at rates of 0.20 and 0.36 Å/cycle at 250 °C, respectively. The crystalline $HfO_2$ and $ZrO_2$ films were etched at 250 °C at rates of 0.02 and 0.18 Å/cycle, respectively. To understand the etching mechanism, the volatile etch products during $HfO_2$ and $ZrO_2$ thermal ALE at 250 °C were identified with high sensitivity quadrupole mass spectrometry (QMS) techniques using $HfO_2$ and $ZrO_2$ powder samples. The QMS studies determined that HF exposures yielded $H_2O$ during fluorination of the metal oxide at 250 °C. After fluorination of $HfO_2$ and $ZrO_2$, QMS analysis identified $Hf(acac)_2F_2$ and $Zr(acac)_2F_2$ etch products, respectively. These mixed ligand fluoro(acetylacetonate) compounds of Hf and Zr have not been reported earlier in the literature. The volatile fluoro(acetylacetonate) compounds appeared immediately with the onset of Hacac exposures. The main $Hf(acac)F_2^+$ and $Zr(acac)F_2^+$ ion intensities from $Hf(acac)_2F_2$ and $Zr(acac)_2F_2$, respectively, also decreased with time during the Hacac exposures. This decrease was consistent with a self-limiting surface reaction. In addition, Hacac exposures on the fluorinated metal oxide surfaces were observed to produce volatile HF at the onset of Hacac exposures at 250 °C. Some of the HF reaction product from the Hacac reaction can potentially return to refluorinate the metal oxide surface and minimize the amount of HF required for additional etching. Experiments with multiple Hacac exposures after the HF fluorination reaction revealed that the $Hf(acac)F_2^+$ and $Zr(acac)F_2^+$ ion intensities decreased progressively with each Hacac exposure after the initial HF exposure. These results confirm that the Hacac reaction is self-limiting even though some HF etch product can remain and refluorinate the $HfO_2$ and $ZrO_2$ surfaces.

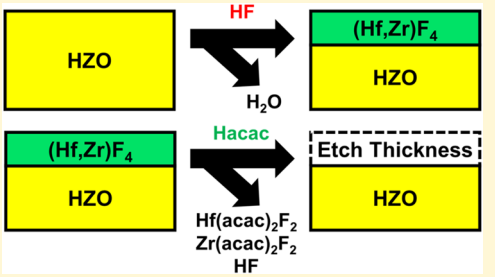


## 1. INTRODUCTION

Atomic layer etching (ALE) is an etch process involving two sequential, self-limiting surface reactions that provides atomic level control of material removal.[1−3] The first reaction involves the modification of the surface of the material. The second step then volatilizes the modified surface layer.[1−3] There are two primary types of ALE: plasma ALE and thermal ALE.[2,3] Plasma ALE usually employs high energy ions to remove the modified surface layer.[2] In contrast, thermal ALE uses thermal reactions to modify the surface layer and remove the surface layer.[1,3]

Multiple mechanisms have been identified for thermal ALE.[3] One pathway is fluorination for surface modification and ligand-exchange for removal of the modified surface layer.[1,3−6] Hydrogen fluoride can be employed for fluorination.[3−5,7] Ligand exchange reactions can then be performed using halogen or methyl exchange reactions.[8−11] This fluorination and ligand-exchange mechanism has been used to etch metal oxides such as $Al_2O_3$,[4,9,12] $HfO_2$,[8,9,13] $ZrO_2$,[9,14] and $Ga_2O_3$.[15]

Another thermal ALE mechanism involves chlorination followed by a ligand addition reaction to volatilize the chlorinated surface layer. This mechanism is effective for etching elemental metals. For example, $SO_2Cl_2$ can be employed for the chlorination of Ni, Co or Au.[16−18] Subsequently, electron-pair donating ligands, such as $P(CH_3)_3$

Received: May 19, 2025
Revised: July 14, 2025
Accepted: July 15, 2025
Published: July 29, 2025

(trimethylphosphine) or $N(CH_3)_2$-$CH_2CH_2N(CH_3)_2$ (tetramethylenediamine), can undergo ligand addition with the metal chloride to form volatile products.[16,17]

Other etching mechanisms for thermal ALE involve the conversion of the top layer of the material to a different material.[19] Subsequently, this conversion reaction is followed by the volatilization of the converted layers.[3,20] Conversion has been reported for $WO_3$ ALE where the $WO_3$ is initially converted to $B_2O_3$ by reaction with $BCl_3$.[20] The $B_2O_3$ layer can then be spontaneously removed by HF exposure.[20,21] Another example is $Al_2O_3$ ALE where $BCl_3$ exposure converts the top layers of $Al_2O_3$ to $B_2O_3$.[22] The $B_2O_3$ is subsequently volatilized by HF exposure.[21,22] Conversion can also be used together with the fluorination and ligand-exchange mechanism for $SiO_2$ and ZnO thermal ALE.[19,23,24]

Acetylacetone (Hacac) and hexafluoroacetylacetone (Hhfac) are effective reactants for etching. Some metal oxides, such as copper oxide, iron oxide, $Mn_2O_3$ and ZnO, can be spontaneously etched using Hacac or Hhfac.[25−29] Consequently, pathways for the ALE of metals can be designed using oxidation and exposure to organics such as formic acid, Hacac or Hhfac.[30,31] The ALE of many elemental metals has been achieved using this strategy.[30,32] Chlorination can also be used together with Hacac or Hhfac for volatilization to etch elemental Co and Fe.[33,34]

The thermal reaction between Hacac and a variety of metal oxides such as $Cr_2O_3$, ZnO, $V_2O_5$, $VO_2$, $Mn_2O_3$, and $Cu_2O$ can form volatile $M(acac)_x$ compounds. This chemical process involves ligand substitution and hydrogen transfer reactions.[35] The acac ligand substitutes for oxygen in the metal oxide. The hydrogen on Hacac transfers to oxygen in the metal oxide to form $H_2O$. The reaction between Hacac and metal oxides can be continuous and produce spontaneous etching. The Hacac reaction can also be limited and used to define ALE strategies. In this case, the Hacac reaction is paired with a surface cleaning reaction using $O_3$ or $O_2$ plasma.[25,35,36]

Hhfac has also been used together with a $H_2$ plasma or O radical exposure to define ALE processes for various metal oxides.[37,38] Because Hhfac contains fluorine, these ALE processes may be fluorinating the metal oxide by decomposition of the adsorbed Hhfac species by the $H_2$ plasma or O radical exposures.[37] Consequently, the volatilization reaction may be between Hhfac and the metal fluoride rather than the metal oxide.

In this paper, we report a ligand substitution and hydrogen transfer mechanism between Hacac and metal fluorides based on a thermal ALE mechanism. The metal fluorides are formed directly in a thermal fluorination reaction of the metal oxide by HF. In the Hacac volatilization reaction, the acac ligand substitutes for fluorine in the metal fluoride. The hydrogen on Hacac transfers to fluorine in the metal fluoride to form HF. The proposed mechanism for HZO thermal ALE using HF and Hacac is shown in Figure 1.

Earlier studies of $HfO_2$ and $ZrO_2$ thermal ALE have utilized other reactions to volatilize the modified fluorinated $HfO_2$ or $ZrO_2$ surface using ligand-exchange reactions. The first report of $HfO_2$ thermal ALE employed HF for fluorination and $Sn(acac)_2$ for ligand exchange.[13] Other demonstrations of $HfO_2$ and $ZrO_2$ thermal ALE used HF for fluorination and $TiCl_4$ or $AlCl(CH_3)_2$ for ligand exchange.[8,9,14,39] $SF_4$ and $XeF_2$ have also been used for fluorination together with $TiCl_4$ or $AlCl(CH_3)_2$ for ligand exchange.[40]

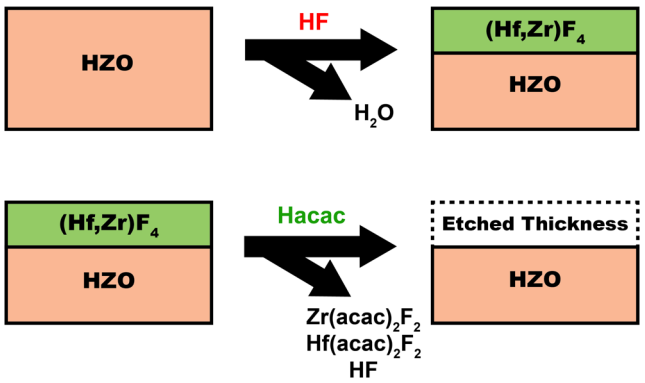


**Figure 1.** Proposed mechanism for HZO thermal ALE using sequential HF and Hacac exposures.

The thermal ALE of HZO, $HfO_2$ and $ZrO_2$ films is important for semiconductor processing. High-*k* ferroelectric materials such as HZO have applications for low power nonvolatile memory devices such as ferroelectric random access memory (FeRAM), ferroelectric field effect transistors (FeFET) and ferroelectric tunnel junctions (FTJ).[41,42] Controlling the ferroelectric film thickness and structure in the sub 10 nm thickness regime is critical for ferroelectric properties.[43]

High-*k* dielectric materials such as HZO, $HfO_2$ and $ZrO_2$ are also useful to fabricate capacitors for DRAM.[44,45] For higher capacitance, these capacitors are usually formed on trench or via structures with a high aspect ratio.[44] Thicker films are easier to crystallize than ultrathin films.[39,40] Using the deposition and etch-back process,[46] ultrathin crystalline films can be obtained by annealing thicker amorphous films and then reducing the crystalline film thickness using ALE.[39,40] Thermal ALE processes are preferred because plasma or radical methods are restricted to small aspect ratio structures resulting from recombination processes.[47,48] In addition, the development of different chemistries for thermal ALE will be useful to obtain selective ALE between HZO, $HfO_2$ and $ZrO_2$ and other materials.[49]

## 2. EXPERIMENTAL METHODS

**2.A. In Situ Spectroscopic Ellipsometry (SE) Experiments.** The in situ SE experiments were conducted in a warm-wall, hot-stage type reactor as described previously.[50] The sample stage temperature was varied between 230 and 270 °C. The walls of the reactor were maintained at 160 °C. The reaction temperature was controlled by the heating of the sample stage using a cartridge heater.

One cycle of HZO thermal ALE consisted of a 5 s dose of HF at 0.5 Torr followed by a 5 s dose of Hacac at 0.4 Torr. Between each dose, there was a 30 s purge using the $N_2$ carrier gas. The $N_2$ carrier gas was flowed at 100 sccm at a base pressure of ∼ 1 Torr. HZO experiments were performed under static conditions. The corresponding $HfO_2$ and $ZrO_2$ experiments were performed under viscous flow conditions. Static and viscous flow conditions should yield the same etch rates when the HF and Hacac reactions are in saturation.

These studies utilized a spectroscopic ellipsometer (J. A. Woollam, model M-2000UI) to monitor changes in film thicknesses. Ψ and Δ were measured from 240 to 1000 nm at an incidence angle of 70°. CompleteEASE software (J. A. Woollam) was used to model the results to determine the thickness and optical constants. Thickness measurements using in situ SE were recorded during the second purge of each cycle to monitor the change in film thickness.

The following fitting layers from J. A. Woollam (JAW) were used to model the film thickness changes. For HZO: HfO2 (TaucLor), TiN_3 (Lorentz), NTVE_JAW (Native Silicon Oxide), and


https://doi.org/10.1021/acs.chemmater.5c01228
Chem. Mater. 2025, 37, 5935−5945

Si_Temp_JAW(−25_500C). For $HfO_2$: HfO2(TaucLor) on NTVE_JAW (20Å, fixed) on Si_Temp_JAW(−25_500C). For $ZrO_2$: ZrO2(Cauchy) on NTVE_JAW (20Å, fixed) on Si_Temp_JAW(−25_500C).

**2.B. Grazing Incidence X-ray Diffraction (GI-XRD) Analysis.** Film crystallinity and crystal phases were determined using grazing incidence X-ray diffraction (GI-XRD). The GI-XRD scans were obtained using an X-ray diffractometer (Bede D1, Jordan Valley Semiconductors) with radiation from the Cu K$\alpha$ line at $\lambda$ = 1.540 Å. The voltage of the X-ray tube filament was 40 kV and the current was 38 mA. The incident angle during GI-XRD was 0.5°.

The amorphous HZO film had a thickness of 10 nm on a TiN film at a thickness of 20 nm deposited on a silicon substrate with a native oxide. The amorphous HZO film was deposited using atomic layer deposition (ALD). The crystalline HZO films were deposited by ALD and then annealed at 400 °C for crystallization. The crystalline HZO films had a thickness of 10 nm. The GI-XRD analysis of the amorphous and crystalline HZO films is displayed in Figure 2a. The majority of the annealed HZO film was in the orthorhombic/tetragonal phase with a small fraction of monoclinic phase.

The XRD analysis of the amorphous and crystalline $HfO_2$ and $ZrO_2$ films is displayed in Figure 2b,c, respectively. The amorphous $HfO_2$ and $ZrO_2$ films with a thickness of 10 nm were deposited using ALD. The crystalline $HfO_2$ and $ZrO_2$ films were deposited using ALD and then annealed for crystallization. The crystalline $HfO_2$ films had a thickness of 18 nm and were monoclinic. The crystalline $ZrO_2$ films were annealed at 800 °C using rapid thermal annealing. These crystalline $ZrO_2$ films had a thickness of 26 nm and were tetragonal/monoclinic.

**2.C. Quadrupole Mass Spectrometry (QMS) Studies.** QMS studies of HZO thermal ALE were performed in a chemical reactor as described previously.[11,50] The reactor contained dual reactant manifolds for alternating doses of the ALE precursors.[50] This design keeps the precursors segregated until they reach the powder bed to prevent cross-contamination of the precursors and minimize potential side reactions. After passing through the nanopowders, the gas phase precursors and etch products were directed via molecular beam expansion through a series of line-of-sight apertures and skimmer toward the ionizer of the mass spectrometer.[11] The gas phase precursors and etch products were then detected by the quadrupole mass spectrometer (Extrel MAX-QMS flange-mounted system).

Nanopowders were used to maximize the surface area. The experiments used $HfO_2$ powders (99.99%, high purity, 61−80 nm, Cubic, US Research Nanomaterials) and $ZrO_2$ powders (99+%, 40 nm, US Research Nanomaterials). Particle sizes ranged from 40 to 80 nm. An average of 29 mg of nanopowder was loaded into the reactor for each experiment.

In each QMS experiment, the combined flow rate of the ultrahigh purity $N_2$ carrier gas through the nested inlet lines was 1.6 sccm. The $N_2$ gas flow produced an average pressure of ∼ 2.8 Torr in the sample holder. This constant $N_2$ flow acts as both a carrier gas for the etch precursors and a purge gas between precursor doses. The HF (70% HF, 30% pyridine, Millipore-Sigma) was dosed at an average partial pressure of ∼ 4.4 Torr for all experiments. The Hacac (≥99%, Millipore-Sigma) was dosed at an average partial pressure of ∼ 3.2 Torr. The experiments were conducted using precursor exposures for 120 s. The precursor exposures were followed by a 300 s purge time to remove excess precursor and etch products from the powder bed by the $N_2$ carrier gas. The temperature of the powder bed was held at 250 °C for all QMS experiments.

The isotopic distributions of each etch product were used to identify the etch products. These isotopic distributions were calculated from the naturally occurring isotopic abundances of each element present in the compounds. For example, Zr has five naturally occurring isotopes: $^{90}Zr$, $^{91}Zr$, $^{92}Zr$, $^{94}Zr$, and $^{96}Zr$. Fluorine, carbon, and oxygen also have significant stable isotopes. Using the known abundances of these isotopes, a simulated mass spectrum was calculated for each etch product. The etch products were confirmed by comparing this simulated spectrum to the observed spectrum. Some $m/z$ values contained signal contributions from more than one chemical species. Deconvolution of the mass peaks in the areas of overlap was needed to properly identify these species.

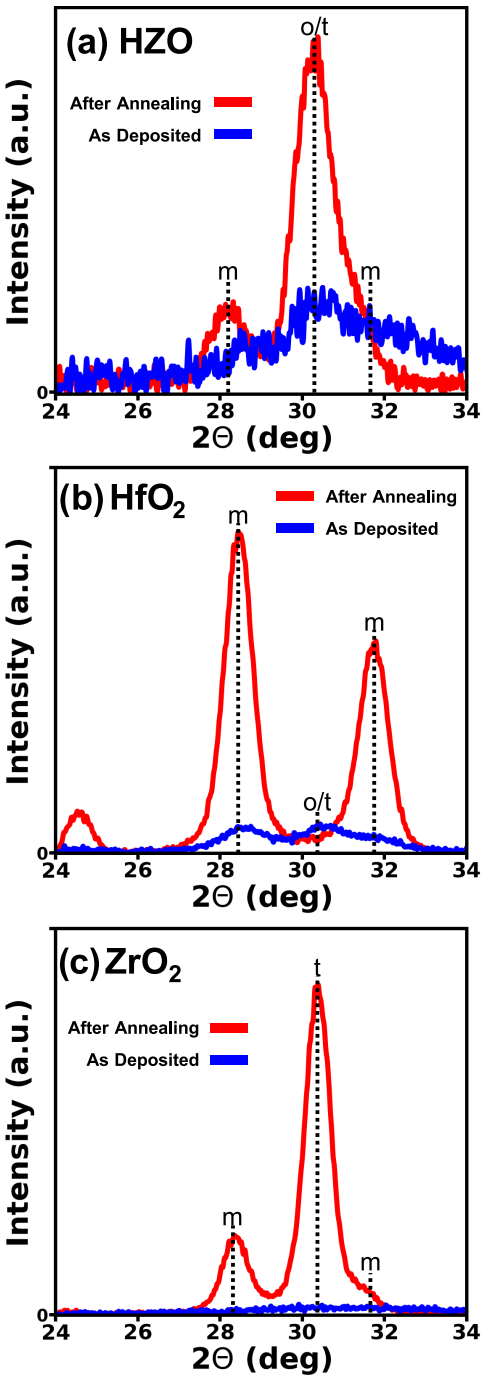


**Figure 2.** GI-XRD analysis of: (a) as deposited and annealed HZO films; (b) as deposited and annealed $HfO_2$ films; and (c) as deposited and annealed $ZrO_2$ films.

**2.D. X-ray Photoelectron Spectroscopy.** X-ray photoelectron spectroscopy (XPS) was performed on the HZO thin films. The X-ray photoelectron spectrometer (PHI 5600) was equipped with a monochromatic A1 K$\alpha$ X-ray source. The resulting XPS data were analyzed using CASA XPS (Casa Software Ltd.) software.

Figure 3 shows the composition of the crystalline HZO film with a film thickness of 10 nm deposited on TiN with a thickness of 20 nm. After sputtering to remove the adventitious carbon, the HZO film contained approximately 54 atom % O, 22 atom % Hf and 22 atom % Zr after a sputter time of 175 s. These percentages are consistent with equal amounts of Hf and Zr and a slightly oxygen-rich stoichiometry.


https://doi.org/10.1021/acs.chemmater.5c01228
Chem. Mater. 2025, 37, 5935−5945

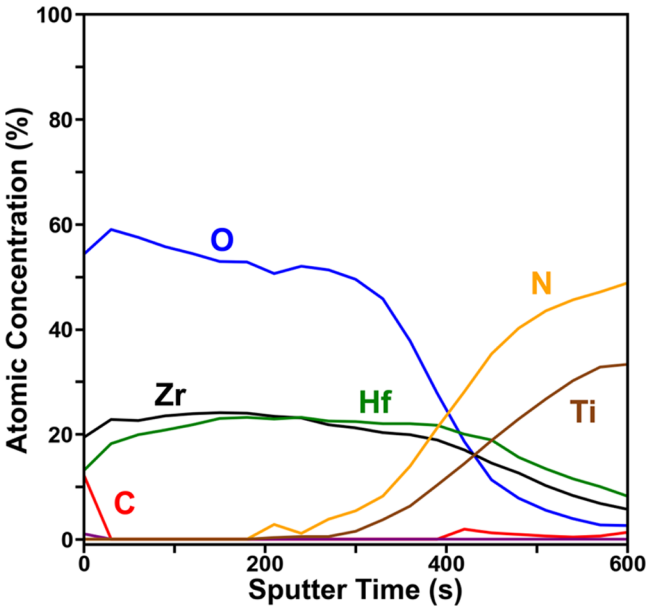


**Figure 3.** XPS analysis of HZO film using sputter depth-profiling. HZO film is approximately 1:1 Hf/Zr deposited on a TiN substrate.

The film was completely removed by sputtering to reveal the underlying TiN substrate. The XPS results for amorphous HZO films were very similar.

## 3. RESULTS AND DISCUSSION

**3.A. HZO Thermal ALE Studied Using In Situ SE.** In situ SE was used to study HZO thermal ALE using HF and Hacac as the reactants. Initial experiments first confirmed that negligible etching occurred using only Hacac and ozone as the reactants.[25] Alternating doses of Hacac and ozone were performed from 210 to 250 °C. No etching was recorded during 60 ALE cycles. Hacac will not spontaneously etch the HZO films. These investigations demonstrated that the fluorination reaction with HF is needed for HZO ALE.

Figure 4 shows the in situ SE results for the change in HZO film thickness versus number of ALE cycles using sequential HF and Hacac exposures. These experiments were performed using 5 s static exposures. The HF exposure was at 0.5 Torr. The Hacac exposure was at 0.4 Torr. There was no observed delay for the etching. The change in film thickness was also linear with number of ALE cycles. The amorphous HZO film etched at a rate of 0.80 Å/cycle at 230 °C. The crystalline HZO films etched at rates of 0.50 and 0.74 Å/cycle at 250 and 270 °C, respectively.

These results are consistent with earlier results for HZO thermal ALE that observed faster etching for amorphous HZO films compared with crystalline HZO films at 250 °C with a variety of fluorination and ligand-exchange precursors.[40] Using $HF/TiCl_4$, $HF/AlCl(CH_3)_2$ (dimethylaluminum chloride (DMAC)), $SF_4/TiCl_4$ and $XeF_2/TiCl_4$ as the reactants, the amorphous HZO films etched at 0.35, 0.69, 0.62, and 2.07 Å/cycle, respectively. In comparison, using $HF/TiCl_4$, HF/DMAC, $SF_4/TiCl_4$ and $XeF_2/TiCl_4$ as the reactants, the crystalline HZO films etched at slower rates of 0.04, 0.16, 0.25, and 1.71 Å/cycle, respectively.[40]

Additional experiments explored the etching of amorphous and crystalline $HfO_2$ films using in situ SE. Figure 5 shows the change in film thickness versus number of ALE cycles for as-deposited $HfO_2$ ALD and annealed $HfO_2$ films at 250 °C.

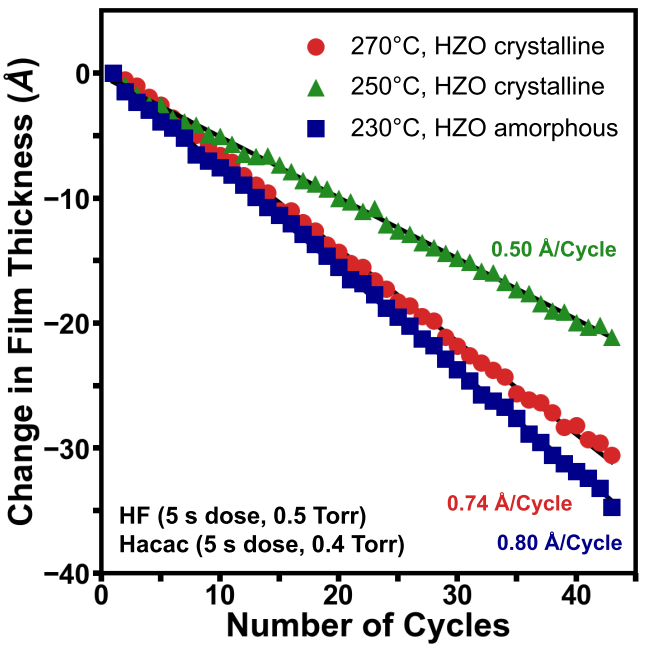


**Figure 4.** Change in HZO film thickness during sequential HF and Hacac exposures on an amorphous HZO film at 230 °C and a crystalline HZO film at 250 and 270 °C. Etch rates were 0.80, 0.50, and 0.74 Å/cycle, respectively.

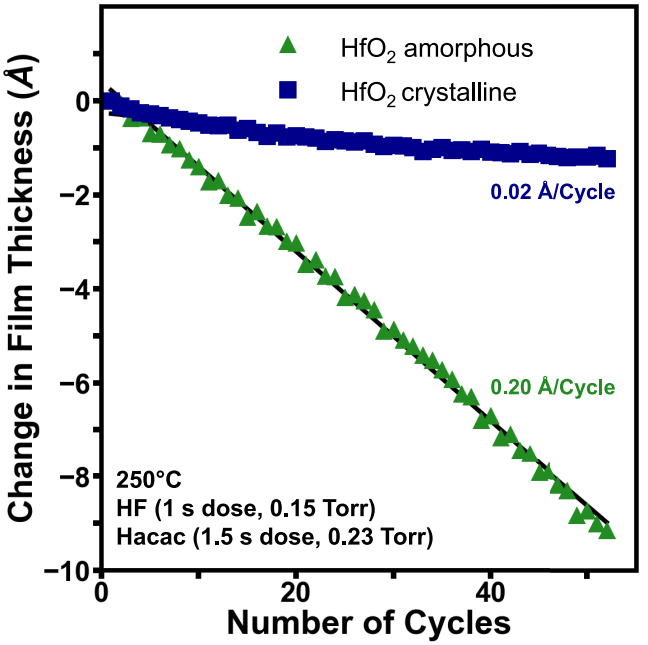


**Figure 5.** Change in $HfO_2$ film thickness during sequential HF and Hacac exposures on amorphous and crystalline $HfO_2$ films at 250 °C. Etch rates were 0.20 and 0.02 Å/cycle, respectively.

These experiments were performed under viscous flow conditions. The HF exposure was 1 s at 0.15 Torr. The Hacac exposure was 1.5 s at 0.23 Torr. There was no delay for the etching. The change in film thickness was also linear with the number of ALE cycles. The amorphous $HfO_2$ ALD film etched at a rate of 0.20 Å/cycle at 250 °C. The annealed crystalline $HfO_2$ film etched at a rate of 0.02 Å/cycle at 250 °C.

These results are in agreement with earlier results for $HfO_2$ thermal ALE that monitored faster etching for amorphous


https://doi.org/10.1021/acs.chemmater.5c01228
Chem. Mater. 2025, 37, 5935−5945

$HfO_2$ films compared with crystalline $HfO_2$ films at 250 °C.[40] Using HF/$TiCl_4$, HF/DMAC, $SF_4$/$TiCl_4$ and $XeF_2$/$TiCl_4$ as the reactants, the amorphous $HfO_2$ films etched at 0.36, 0.68, 0.70, and 1.96 Å/cycle, respectively. In comparison, using HF/$TiCl_4$, HF/DMAC, $SF_4$/$TiCl_4$ and $XeF_2$/$TiCl_4$ as the reactants, the crystalline $HfO_2$ films etched at slower rates of 0.02, 0.08, 0.08, and 1.26 Å/cycle, respectively.[40]

Experiments also examined the etching of amorphous and crystalline $ZrO_2$ films using in situ SE. Figure 6 shows the

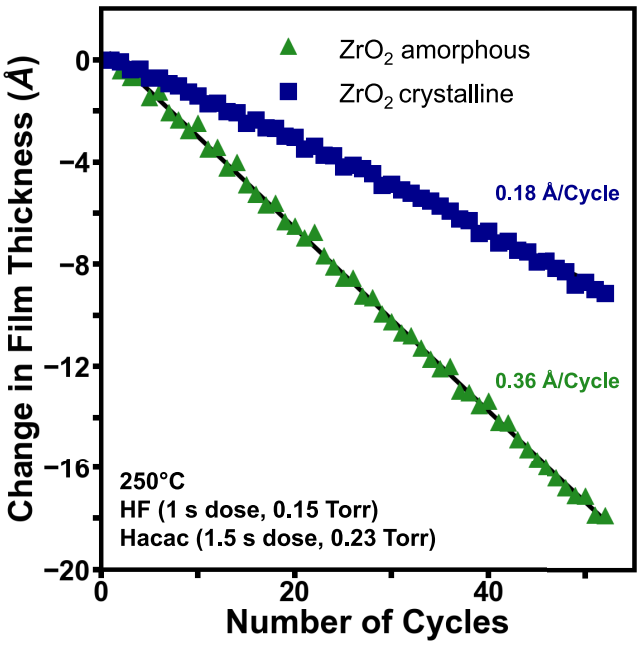


**Figure 6.** Change in $ZrO_2$ film thickness during sequential HF and Hacac exposures on amorphous and crystalline $ZrO_2$ films at 250 °C. Etch rates were 0.36 and 0.18 Å/cycle, respectively.

change in film thickness versus number of ALE cycles for as-deposited $ZrO_2$ ALD and annealed $ZrO_2$ films at 250 °C. Like the experiments for $HfO_2$ thermal ALE shown in Figure 5, these experiments were performed under viscous flow conditions. The HF exposure was 1 s at 0.15 Torr and the Hacac exposure was 1.5 s at 0.23 Torr. The change in film thickness was again linear with the number of ALE cycles. The amorphous $ZrO_2$ ALD film etched at a rate of 0.36 Å/cycle at 250 °C. The annealed crystalline $ZrO_2$ film etched at a rate of 0.18 Å/cycle at 250 °C.

These results are also consistent with earlier results for $ZrO_2$ thermal ALE that measured faster etching for amorphous $ZrO_2$ films compared with crystalline $ZrO_2$ films.[40] Using HF/$TiCl_4$, HF/DMAC, $SF_4$/$TiCl_4$ and $XeF_2$/$TiCl_4$ as the reactants, the amorphous $ZrO_2$ films etched at 0.61, 1.11, 1.08, and 2.69 Å/cycle, respectively. In comparison, using HF/$TiCl_4$, HF/DMAC, $SF_4$/$TiCl_4$ and $XeF_2$/$TiCl_4$ as the reactants, the crystalline $ZrO_2$ films etched at slower rates of 0.26, 0.82, 0.36, and 1.75 Å/cycle, respectively.[40]

The amorphous films may etch faster than the crystalline films because they have lower density.[40,51] This lower density may be able to better accommodate the large volume expansion that occurs during fluorination. For example, the molar volume of crystalline $HfO_2$ is 21.75 $cm^3$/mol.[40] In contrast, the molar volume of crystalline $HfF_4$ is 35.84 $cm^3$/mol.[40] The volume expansion occurring during fluorination of $HfO_2$ to $HfF_4$ is 1.65.[40] The thickness of the fluoride layer may be larger for the lower density amorphous films. These larger fluoride layer thicknesses may then produce higher etch rates.[7] In addition, amorphous materials are generally more reactive than crystalline materials because they have a greater degree of disorder and a larger variation in coordination numbers.

**3.B. $HfO_2$ Thermal ALE Studied Using QMS.** The in situ SE experiments confirm that HZO, $HfO_2$ and $ZrO_2$ films can be etched using fluorination with HF and volatilization with Hacac. QMS was subsequently employed to determine the volatile etch products to verify the etching mechanism shown in Figure 1. In the absence of high surface area HZO powders, these experiments were conducted using $HfO_2$ and $ZrO_2$ powders at 250 °C.

Sequential exposures of HF and Hacac were performed on $HfO_2$ powder at 250 °C. Figure 7 shows the QMS ion signal

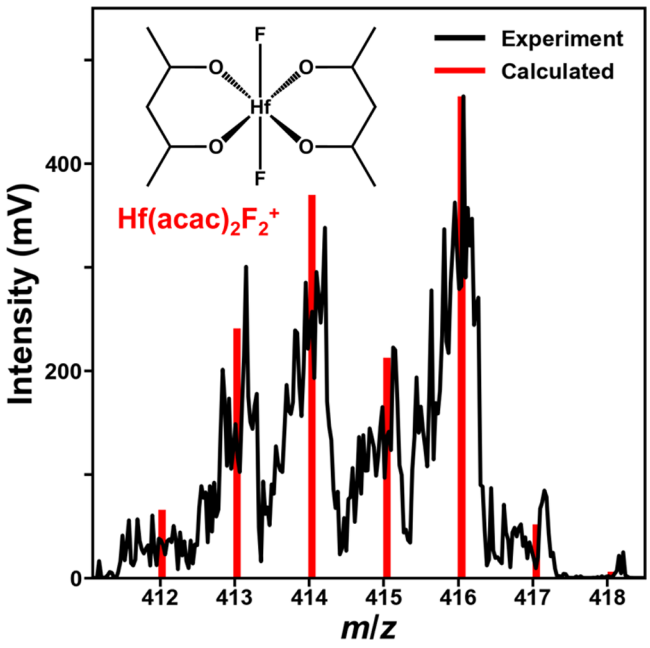


**Figure 7.** Mass spectrum during Hacac exposure on fluorinated $HfO_2$ powder at 250 °C compared with the simulated mass spectrum of $Hf(acac)_2F_2$.

intensity of the etch product, $Hf(acac)_2F_2$, observed during Hacac exposure on fluorinated $HfO_2$ powder. The calculated spectrum of $Hf(acac)_2F_2$ based on natural isotopic abundances is also shown for comparison. The excellent agreement between the experimental and calculated intensities versus $m/z$ confirms $Hf(acac)_2F_2$ as the etch product.

There was no detection of $Hf(acac)_4$ etch product or any other possible $Hf(acac)_xF_y$ etch product. No mass signals were observed at $m/z$ 576 or $m/z$ 496, corresponding to $Hf(acac)_4^+$ or $Hf(acac)_3F^+$, respectively. Furthermore, no mass signals were observed at $m/z$ 477 corresponding to $Hf(acac)_3^+$. Mass signal at $m/z$ 477 for $Hf(acac)_3^+$ is expected to be a major mass fragment for both $Hf(acac)_4^+$ and $Hf(acac)_3F^+$.

The most intense ion intensity at $m/z$ 416 in Figure 7 can be assigned to $^{180}Hf(acac)_2F_2$. The moderately intense peaks at $m/z$ 413, 414, and 415 can be attributed to $^{177}Hf(acac)_2F_2$, $^{178}Hf(acac)_2F_2$, and $^{179}Hf(acac)_2F_2$, respectively. The small $m/z$ 412 peak can be identified as $^{176}Hf(acac)_2F_2$. The


https://doi.org/10.1021/acs.chemmater.5c01228
Chem. Mater. 2025, 37, 5935−5945

additional small peak at $m/z$ 417 can be attributed to the presence of $^{13}C$ in $^{180}Hf(acac)_2F_2$.

$Hf(acac)_4$ is a well-known homoleptic hafnium acetylacetonate. Other mixed ligand hafnium halo(acetylacetonates) have also been reported such as $Hf(acac)_2Cl_2$, $Hf(acac)_2Br_2$, $Hf(acac)_3Cl$, and $Hf(acac)_3Br$.[52−54] However, there have been no previous reports of hafnium fluoro(acetylacetonates) such as $Hf(acac)_2F_2$ to our knowledge. This observation of $Hf(acac)_2F_2$ as the hafnium-containing etch product from $HfO_2$ ALE using HF and Hacac as the reactants is the first known identification of $Hf(acac)_2F_2$. Reports of fluoro(acetylacetonate) metal complexes are much less common than chloro(acetylacetonate) and bromo(acetylacetonate) metal complexes.

Based on the proposed etch mechanism shown in Figure 1, the reaction of Hacac with fluorinated $HfO_2$ could form $Hf(acac)_2F_2$ according to

$$HfF_4 + 2Hacac(g) \rightarrow Hf(acac)_2F_2(g) + 2HF(g) \quad (1)$$

This reaction pathway is based on ligand substitution and hydrogen transfer by Hacac. Acac substitutes for fluorine on $HfF_4$. The hydrogen from Hacac transfers to fluorine to form HF. The appearance of HF as an etch product is unusual because HF is also the fluorination reactant in the surface modification reaction. This HF etch product could refluorinate the underlying $HfO_2$ substrate.

QMS studies can also confirm the fluorination of $HfO_2$ by HF. Figure 8a reveals that $H_2O$ is produced during the HF exposure on initial $HfO_2$ powder prior to any Hacac exposure. This reaction is expected because fluorination of $HfO_2$ by HF is thermochemically favorable.[55]

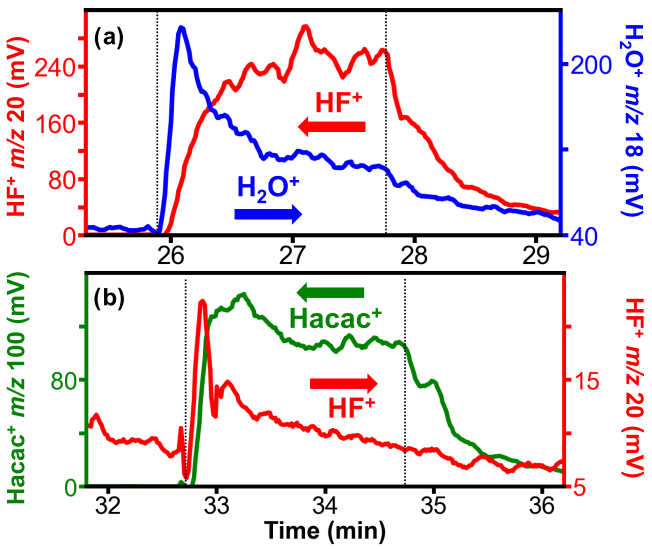


**Figure 8.** (a) $H_2O^+$ and $HF^+$ ion intensities versus time during HF exposure on initial $HfO_2$ powder prior to any Hacac exposure at 250 °C. (b) $HF^+$ and $Hacac^+$ ion intensities versus time during Hacac exposure on fluorinated $HfO_2$ powder at 250 °C. Vertical dashed lines indicate the beginning and end of the reactant exposures.

$$HfO_2 + 4HF(g) \rightarrow HfF_4 + 2H_2O(g)$$
$$\Delta G^\circ(250\ ^\circ C) = -16.4\ kcal \quad (2)$$

The $H_2O^+$ ion intensity is observed at the beginning of the HF exposure. In addition, $H_2O$ is evolved before the appearance of the HF reactant. This observation indicates that most of the HF precursor is consumed by the fluorination reaction as HF fluorinates the $HfO_2$ surface. As the fluorination reaction reaches saturation, the $H_2O^+$ ion intensity decreases and the $HF^+$ ion intensity rises. This behavior is consistent with a self-limiting fluorination reaction.

The QMS investigations can also determine if Hacac exposure on the fluorinated $HfO_2$ surface yields volatile HF as an etch product. Figure 8b shows that $HF^+$ ion intensity is observed at the beginning of the Hacac exposure on the fluorinated $HfO_2$ powder. This volatile HF etch product is consistent with hydrogen transfer from Hacac to fluorine on the fluorinated $HfO_2$ powder. In addition to the volatile HF etch product, additional HF etch product could remain and refluorinate the underlying $HfO_2$ surface. Figure 8b reveals that the $Hacac^+$ ion intensity increases as the $HF^+$ ion intensity decreases. The $Hacac^+$ ion intensity is then constant throughout the remainder of the Hacac exposure.

QMS experiments can also monitor the evolution of the $Hf(acac)_2F_2$ etch product versus the Hacac exposure. These studies can determine if the volatilization reaction displays self-limiting behavior. Figure 9 displays the $Hf(acac)F_2^+$ ion intensity during an Hacac exposure on the fluorinated $HfO_2$ powder. The $Hf(acac)F_2^+$ ion intensity was selected to monitor the parent $Hf(acac)_2F_2^+$ ion intensity because this fragment has a signal intensity about 6 times higher than the parent $Hf(acac)_2F_2^+$ ion intensity. The $Hf(acac)F_2^+$ ion signal was also observed to scale with the $Hf(acac)_2F_2^+$ parent ion signal over the course of the experiments.

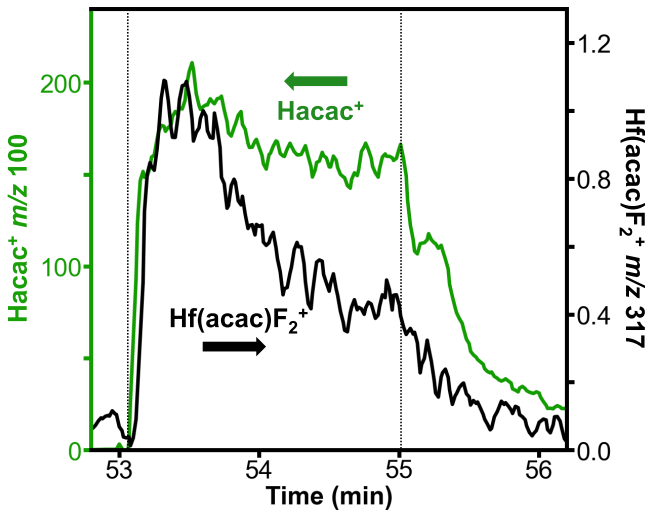


**Figure 9.** $Hf(acac)F_2^+$ and $Hacac^+$ ion intensities versus time during Hacac exposure on fluorinated $HfO_2$ powder at 250 °C. Vertical dashed lines indicate the beginning and end of the reactant exposures.

Figure 9 shows that the $Hf(acac)F_2^+$ signal has its highest intensity at the beginning of the Hacac exposure. The $Hf(acac)F_2^+$ ion intensity then decreases while the $Hacac^+$ ion intensity remains constant. This behavior indicates that the Hacac can spontaneously etch the fluorinated $HfO_2$ surface. However, as the fluorinated layer is removed by the reaction, the $Hf(acac)_2F_2$ etch product progressively decreases. These results are consistent with a self-limiting reaction between Hacac and the fluorinated layer on the $HfO_2$ surface.

The evolution of $HfO_2$ thermal ALE during HF and Hacac exposures can also be monitored with QMS studies. Figure 10


https://doi.org/10.1021/acs.chemmater.5c01228
Chem. Mater. 2025, 37, 5935−5945

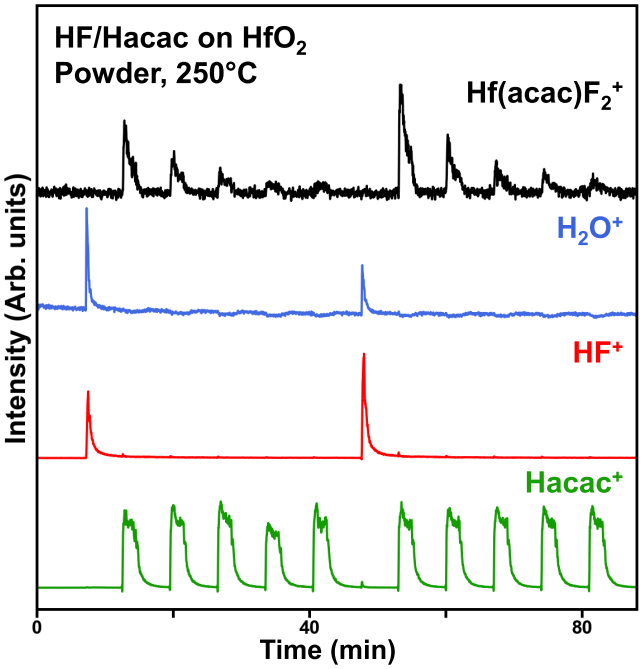


**Figure 10.** Ion intensities for $Hf(acac)F_2^+$, $H_2O^+$, $HF^+$ and $Hacac^+$ versus time for single HF exposures followed by five successive Hacac exposures on $HfO_2$ powders at 250 °C.

shows time-resolved QMS results during an HF exposure and multiple Hacac exposures. Initially, the first HF exposure on fresh $HfO_2$ powder yields $H_2O$ as anticipated from Figure 8a. The subsequent five successive Hacac exposures all produce $Hf(acac)F_2^+$ ion intensity. However, the size of the $Hf(acac)F_2^+$ ion intensity decreases with each Hacac exposure as expected for a self-limiting reaction. The next HF exposure again produces $H_2O$. The following five successive Hacac exposures again produce $Hf(acac)F_2^+$ ion intensity that decreases progressively with each Hacac exposure.

Following fluorination by HF, there are small $HF^+$ ion intensities that are monitored in Figure 10 on the rising edge of the Hacac exposures in agreement with Figure 8b. However, these $HF^+$ ion intensities are weak in comparison with the $HF^+$ reactant ion intensities. The $HF^+$ ion intensities also decrease progressively with each Hacac exposure. The decrease is similar to the decrease in the $Hf(acac)F_2^+$ ion intensity with each Hacac exposure. This progressive decrease is consistent with a self-limiting reaction between Hacac and the fluorinated $HfO_2$ surface and the decreasing refluorination of the underlying $HfO_2$ surface by the HF etch productt. Progressively smaller amounts of HF etch product would be available to refluorinate the $HfO_2$ surface during each Hacac exposure because HF etch product is also lost to the gas phase.

Figure 10 also shows a large $H_2O^+$ ion signal that coincides with the first HF reactant exposure on fresh $HfO_2$ powder. Subsequently, the second HF reactant exposure produces a smaller $H_2O^+$ ion signal. This behavior is explained by the more complete consumption of HF during fluorination of the fresh $HfO_2$ powder. This initial fluorination produces a large $H_2O^+$ ion signal. The second HF reactant exposure is then not consumed as much by the previously fluorinated $HfO_2$ powder. This smaller consumption of HF leads to a larger $HF^+$ ion signal and a correspondingly smaller $H_2O^+$ ion signal. However, the second HF reactant exposure may lead to a higher degree of fluorination of the $HfO_2$ powder. This more complete fluorination of the $HfO_2$ powder may explain the higher $Hf(acac)F_2^+$ ion signal observed during the next Hacac exposure.

**3.C. $ZrO_2$ Thermal ALE Studied Using QMS.** Sequential exposures of HF and Hacac were also conducted on $ZrO_2$ powder at 250 °C. Figure 11 displays the QMS ion signal

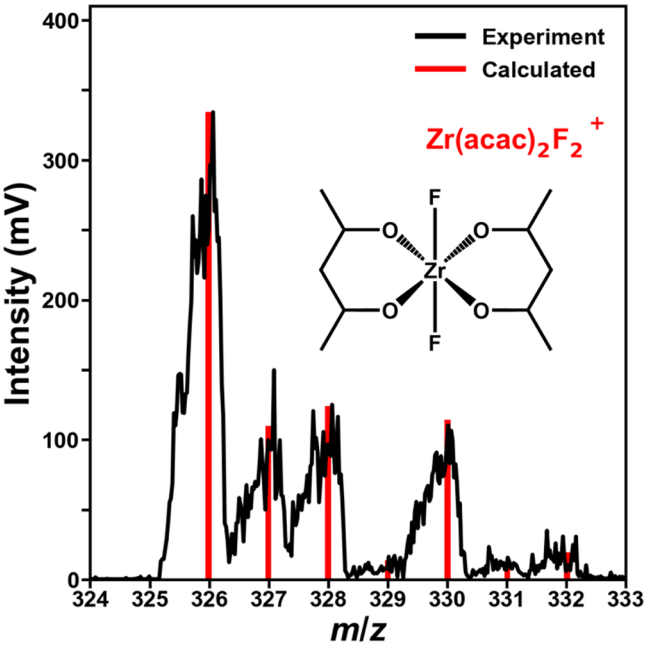


**Figure 11.** Mass spectrum during Hacac exposure on fluorinated $ZrO_2$ powder at 250 °C compared with the simulated mass spectrum of $Zr(acac)_2F_2$.

intensity of the etch product, $Zr(acac)_2F_2$, monitored during Hacac exposure on fluorinated $ZrO_2$ powder. The calculated spectrum of $Zr(acac)_2F_2$ based on natural isotopic abundances is also shown for comparison. In similarity with the results for $Hf(acac)_2F_2$ in Figure 7, there is agreement between the experimental and calculated intensities that confirms $Zr(acac)_2F_2$ as the etch product.

The primary ion intensity at $m/z$ 326 in Figure 11 is attributed to $^{90}Zr(acac)_2F_2$. The three smaller signals at $m/z$ 327, 328, and 330 are attributed to $^{91}Zr(acac)_2F_2$, $^{92}Zr(acac)_2F_2$, and $^{94}Zr(acac)_2F_2$, respectively. The very low signal at $m/z$ 332 is attributed to $^{96}Zr(acac)_2F_2$. The small signals at $m/z$ 329 and 331 are from the presence of $^{13}C$ in the acetylacetonate ligands. There was no detection of the possible $Zr(acac)_4$ etch product or any other $Zr(acac)_xF_y$ etch product. No mass signals were observed at $m/z$ 486 or $m/z$ 416, corresponding to $Zr(acac)_4^+$ or $Zr(acac)_3F^+$, respectively. Furthermore, no mass signals were observed at $m/z$ 387 corresponding to $Zr(acac)_3^+$. Mass signal at $m/z$ 387 for $Zr(acac)_3^+$ is expected to be a major mass fragment for both $Zr(acac)_4^+$ and $Zr(acac)_3F^+$.

The most common zirconium acetylacetonate is $Zr(acac)_4$. Other mixed ligand zirconium halo(acetylacetonates) have also been documented such as $Zr(acac)_2Cl_2$, $Zr(acac)_2Br_2$, $Zr(acac)Cl_3$, $Zr(acac)_3Br$, and $Zr(acac)_3I$.[52−54] $Zr(acac)_2Cl_2$ is reported frequently in the literature because of its role in olefin polymerization as a Ziegler−Natta catalyst.[56,57] However, no previous reports of $Zr(acac)_2F_2$ exist to our knowledge. The detection of $Zr(acac)_2F_2$ as an etch product


https://doi.org/10.1021/acs.chemmater.5c01228
Chem. Mater. 2025, 37, 5935−5945

from $ZrO_2$ ALE using HF and Hacac as the reactants is the first known identification of $Zr(acac)_2F_2$. In similarity with the reaction of Hacac with fluorinated $HfO_2$, the reaction of Hacac with fluorinated $ZrO_2$ could form $Zr(acac)_2F_2$ based on ligand substitution and hydrogen transfer:

$$ZrF_4 + 2Hacac(g) \rightarrow Zr(acac)_2F_2(g) + 2HF(g) \quad (3)$$

Additional QMS studies were performed to confirm the reactions occurring during $ZrO_2$ ALE. In similarity with Figure 8a, Figure 12a reveals that $H_2O$ is produced during HF exposure on initial $ZrO_2$ powder prior to any Hacac exposure. This reaction is anticipated because fluorination of $ZrO_2$ by HF is thermochemically favorable.[55]

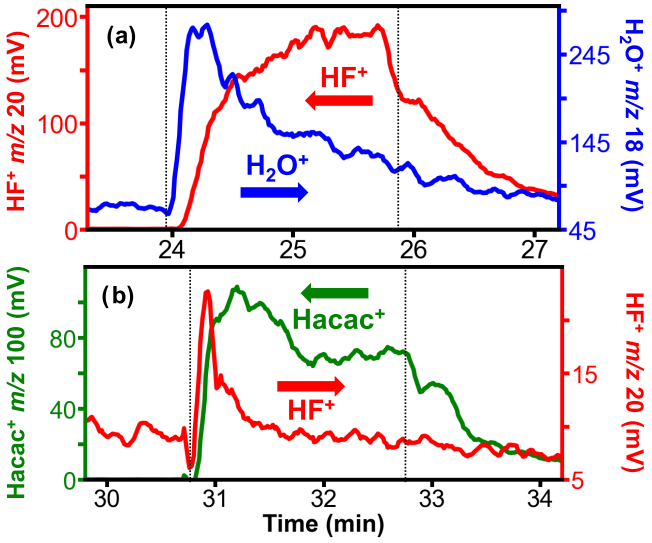


**Figure 12.** (a) $H_2O^+$ and $HF^+$ ion intensities versus time during HF exposure on initial $ZrO_2$ powder prior to any Hacac exposure at 250 °C. (b) $HF^+$ and $Hacac^+$ ion intensities versus time during Hacac exposure on fluorinated $ZrO_2$ powder at 250 °C. Vertical dashed lines indicate the beginning and end of the reactant exposures.

$$ZrO_2 + 4HF(g) \rightarrow ZrF_4 + 2H_2O(g)$$
$$\Delta G^\circ(250\ ^\circ C) = -15.2\ kcal \quad (4)$$

The $H_2O^+$ ion intensity is observed at the beginning of the HF exposure. As the $H_2O^+$ ion intensity decreases, the $HF^+$ ion intensity rises. This observation is consistent with a self-limiting fluorination reaction.

QMS investigations also determined if Hacac exposure on the fluorinated $ZrO_2$ surface yielded HF as an etch product. In similarity with Figure 8b, Figure 12b shows that $HF^+$ ion intensity is observed at the beginning of the Hacac exposure on the fluorinated $ZrO_2$ powder. In addition to this volatile HF etch product, additional HF etch product could remain and refluorinate the underlying $ZrO_2$ surface. Figure 12b also reveals that the $Hacac^+$ ion intensity increases as the $HF^+$ ion intensity decreases.

QMS experiments also monitored the evolution of the $Zr(acac)_2F_2$ etch product versus the Hacac exposure. Figure 13 shows the $Zr(acac)F_2^+$ ion intensity during an Hacac exposure on the fluorinated $ZrO_2$ powder. The $Zr(acac)F_2^+$ ion intensity was used to monitor the parent $Zr(acac)_2F_2^+$ ion intensity because this fragment has a signal intensity about 10 times higher than the parent $Zr(acac)_2F_2^+$ ion intensity. The

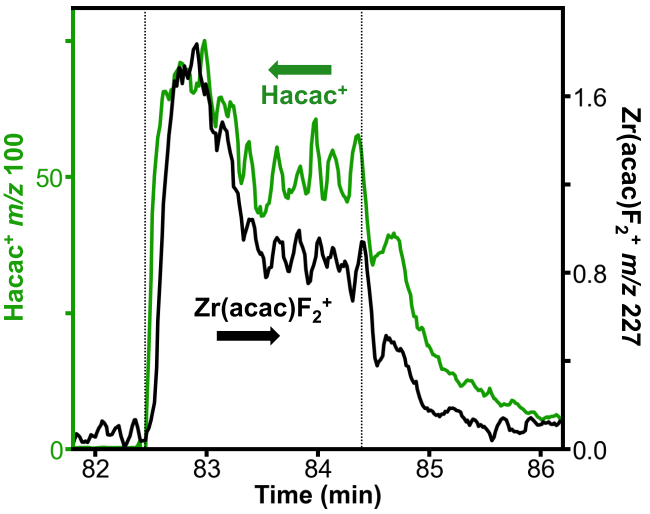


**Figure 13.** $Hf(acac)F_2^+$ and $Hacac^+$ ion intensities versus time during Hacac exposure on fluorinated $ZrO_2$ powder at 250 °C. Vertical dashed lines indicate the beginning and end of the reactant exposures.

$Zr(acac)F_2^+$ ion intensity decreases while the $Hacac^+$ ion intensity remains fairly constant. This behavior suggests that the $Zr(acac)_2F_2$ etch product decreases as the fluorinated layer is removed by the Hacac reaction. However, the results in Figure 13 do not argue as strongly for a self-limiting reaction as the results in Figure 9 for Hacac reacting with the fluorinated $HfO_2$ powder.

Although the results in Figure 13 did not clearly support a self-limiting reaction, the QMS results during an HF exposure and multiple Hacac exposures on $ZrO_2$ powders are more definite. Figure 14 shows that the first HF exposure on fresh $HfO_2$ powder yields $H_2O$ as expected from Figure 12a. The next five successive Hacac exposures all produce $Zr(acac)F_2^+$

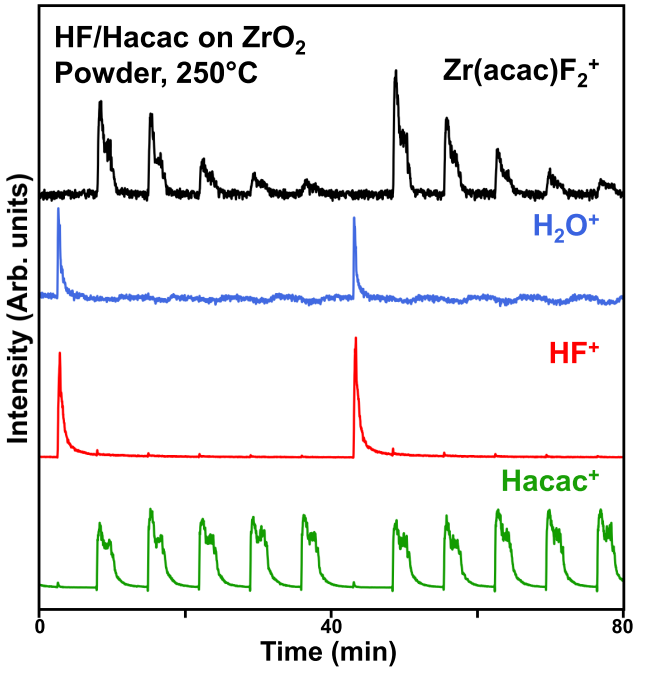


**Figure 14.** Ion intensities for $Zr(acac)F_2^+$, $H_2O^+$, $HF^+$ and $Hacac^+$ versus time for single HF exposures followed by five successive Hacac exposures on $ZrO_2$ powders at 250 °C.


https://doi.org/10.1021/acs.chemmater.5c01228
Chem. Mater. 2025, 37, 5935−5945

ion intensity. However, the size of the $Zr(acac)F_2^+$ ion intensity decreases with each Hacac exposure. This behavior is expected for a self-limiting reaction.

The subsequent HF exposure in Figure 14 again produces $H_2O$. The following five successive Hacac exposures then produce $Zr(acac)F_2^+$ ion intensity that decreases progressively with each Hacac exposure. These decreasing $Zr(acac)F_2^+$ ion intensities confirm self-limiting behavior. In similarity with the results for the $HF^+$ ion intensities in Figure 10, there are also small $HF^+$ ion intensities that are monitored in Figure 14 on the rising edge of the Hacac exposures in agreement with Figure 12b. This gaseous HF etch product observed during Hacac exposures may indicate that other HF etch products that are not volatilized can return and refluorinate the $ZrO_2$ surface. The progressive reduction of the $Zr(acac)F_2^+$ ion intensities may occur because volatile HF is also lost during each Hacac exposure. Less refluorination by HF etch products is possible with each successive Hacac exposure.

## 4. CONCLUSIONS

Sequential HF and Hacac exposures were utilized for HZO, $HfO_2$ and $ZrO_2$ thermal ALE. HF modifies the metal oxide surface by forming a metal fluoride layer. Hacac then reacts with the metal fluoride layer to form volatile products by a ligand substitution and hydrogen transfer reaction. The ligand substitution reaction produces volatile metal acac complexes. The hydrogen transfer reaction produces an HF etch product. This HF etch product could be lost as volatile HF or could remain and refluorinate the underlying metal oxide

High sensitivity QMS experiments on $HfO_2$ and $ZrO_2$ powder samples showed that the HF exposures yielded $H_2O$ during fluorination of the metal oxide at 250 °C. After fluorination, QMS analysis revealed that Hacac exposures produced $Hf(acac)_2F_2$ and $Zr(acac)_2F_2$ etch products. This is the first known report of these mixed ligand fluoro(acetylacetonate) Hf and Zr compounds. These volatile mixed ligand fluoro(acetylacetonate) compounds appeared immediately with the Hacac exposures on fluorinated $HfO_2$ and $ZrO_2$ powder samples. The decrease of these mixed ligand fluoro(acetylacetonate) compounds with time during the Hacac exposure was also consistent with a self-limiting surface reaction.

QMS analysis also revealed that the Hacac exposures on fluorinated metal oxide surfaces produced HF at the beginning of the Hacac exposures at 250 °C. This HF etch product is unusual because this etch product is also the reactant during the fluorination reaction. In addition to the volatile HF that is detected by the QMS measurements, there also could be product HF that returns to refluorinate the metal oxide surface. This refluorination could recycle some of the original HF used to fluorinate the metal oxides. QMS experiments with multiple successive Hacac exposures after an initial HF exposure revealed that the $Hf(acac)F_2^+$ and $Zr(acac)F_2^+$ ion intensities decreased with each Hacac exposure. These results argue for self-limiting reactions between Hacac and the fluorinated metal oxide surfaces.

In situ spectroscopic ellipsometry investigations confirmed the etching of amorphous and crystalline HZO, $HfO_2$ and $ZrO_2$ films by sequential HF and Hacac exposures. The etch rates of the amorphous films were larger than the etch rates of the crystalline films. Amorphous HZO etched at a rate of 0.80 Å/cycle at 230 °C. In contrast, crystalline HZO was etched at rates of 0.50 and 0.74 Å/cycle at 250 and 270 °C, respectively. Amorphous $HfO_2$ and $ZrO_2$ films were etched at rates of 0.20 and 0.36 Å/cycle at 250 °C, respectively. In comparison, the crystalline $HfO_2$ and $ZrO_2$ ALD films were etched at 250 °C at rates of 0.02 and 0.18 Å/cycle, respectively.

## AUTHOR INFORMATION


### Corresponding Author

**Steven M. George** − *Department of Chemistry, University of Colorado, Boulder, Colorado 80309, United States;* orcid.org/0000-0003-0253-9184; Email: Steven.George@Colorado.edu

### Authors

**Troy A. Colleran** − *Department of Chemistry, University of Colorado, Boulder, Colorado 80309, United States*

**Aziz I. Abdulagatov** − *Department of Chemistry, University of Colorado, Boulder, Colorado 80309, United States*

**Jonathan L. Partridge** − *Department of Chemistry, University of Colorado, Boulder, Colorado 80309, United States;* orcid.org/0000-0002-0071-9854

**Andrew S. Cavanagh** − *Department of Chemistry, University of Colorado, Boulder, Colorado 80309, United States;* orcid.org/0000-0002-6201-530X

Complete contact information is available at: https://pubs.acs.org/10.1021/acs.chemmater.5c01228


### Notes

The authors declare no competing financial interest.

## ACKNOWLEDGMENTS

This work was supported by the Joint University Microelectronics Program (JUMP) funded by the Semiconductor Research Corporation (SRC). Lam Research contributed funding for the QMS reactor and the QMS investigations.

## REFERENCES


(1) Fischer, A.; Routzahn, A.; George, S. M.; Lill, T. Thermal Atomic Layer Etching: A Review. *J. Vac. Sci. Technol., A* **2021**, *39*, No. 030801.

(2) Kanarik, K. J.; Lill, T.; Hudson, E. A.; Sriraman, S.; Tan, S.; Marks, J.; Vahedi, V.; Gottscho, R. A. Overview of Atomic Layer Etching in the Semiconductor Industry. *J. Vac. Sci. Technol., A* **2015**, *33*, No. 020802.

(3) George, S. M. Mechanisms of Thermal Atomic Layer Etching. *Acc. Chem. Res.* **2020**, *53*, 1151−1160.

(4) Lee, Y.; DuMont, J. W.; George, S. M. Mechanism of Thermal $Al_2O_3$ Atomic Layer Etching Using Sequential Reactions with $Sn(acac)_2$ and HF. *Chem. Mater.* **2015**, *27*, 3648−3657.

(5) Lee, Y.; DuMont, J. W.; George, S. M. Trimethylaluminum as the Metal Precursor for the Atomic Layer Etching of $Al_2O_3$ Using Sequential, Self-Limiting Thermal Reactions. *Chem. Mater.* **2016**, *28*, 2994−3003.

(6) George, S. M.; Lee, Y. Prospects for Thermal Atomic Layer Etching Using Sequential, Self-Limiting Fluorination and Ligand-Exchange Reactions. *ACS Nano* **2016**, *10*, 4889−4894.

(7) Cano, A. M.; Marquardt, A. E.; DuMont, J. W.; George, S. M. Effect of HF Pressure on Thermal $Al_2O_3$ Atomic Layer Etch Rates and $Al_2O_3$ Fluorination. *J. Phys. Chem. C* **2019**, *123*, 10346−10355.

(8) Lee, Y.; George, S. M. Thermal Atomic Layer Etching of $HfO_2$ Using HF For Fluorination and $TiCl_4$ For Ligand-Exchange. *J. Vac. Sci. Technol., A* **2018**, *36*, No. 061504.

(9) Lee, Y.; George, S. M. Thermal Atomic Layer Etching of $Al_2O_3$, $HfO_2$, and $ZrO_2$ Using Sequential Hydrogen Fluoride and Dimethylaluminum Chloride Exposures. *J. Phys. Chem. C* **2019**, *123*, 18455−18466.

(10) Lii-Rosales, A.; Johnson, V. L.; Cavanagh, A. S.; Fischer, A.; Lill, T.; Sharma, S.; George, S. M. Effectiveness of Different Ligands on Silane Precursors for Ligand Exchange to Etch Metal Fluorides. *Chem. Mater.* **2022**, *34*, 8641−8653.
(11) Lii-Rosales, A.; Cavanagh, A. S.; Fischer, A.; Lill, T.; George, S. M. Spontaneous Etching of Metal Fluorides Using Ligand-Exchange Reactions: Landscape Revealed by Mass Spectrometry. *Chem. Mater.* **2021**, *33*, 7719−7730.
(12) Lee, Y.; George, S. M. Atomic Layer Etching of $Al_2O_3$ Using Sequential, Self-Limiting Thermal Reactions with $Sn(acac)_2$ and Hydrogen Fluoride. *ACS Nano* **2015**, *9*, 2061−2070.
(13) Lee, Y.; DuMont, J. W.; George, S. M. Atomic Layer Etching of $HfO_2$ Using Sequential, Self-Limiting Thermal Reactions with $Sn(acac)_2$ and HF. *ECS J. Solid State Sci. Technol.* **2015**, *4*, N5013−N5022.
(14) Sempel, J. D.; Kaariainen, M. L.; Colleran, T. A.; Lifschitz, A. M.; George, S. M. Ultrathin $ZrO_2$ Thickness Control on $TiO_2/ZrO_2$ Core/Shell Nanoparticles Using $ZrO_2$ Atomic Layer Deposition and Etching. *J. Vac. Sci. Technol. A* **2024**, *42*, No. 052604.
(15) Lee, Y.; Johnson, N. R.; George, S. M. Thermal Atomic Layer Etching of Gallium Oxide Using Sequential Exposures of HF and Various Metal Precursors. *Chem. Mater.* **2020**, *32*, 5937−5948.
(16) Murdzek, J. A.; Lii-Rosales, A.; George, S. M. Thermal Atomic Layer Etching of Nickel Using Sequential Chlorination and Ligand-Addition Reactions. *Chem. Mater.* **2021**, *33*, 9174−9183.
(17) Murdzek, J. A.; Lii-Rosales, A.; George, S. M. Thermal Atomic Layer Etching of Cobalt Using Sulfuryl Chloride for Chlorination and Tetramethylethylenediamine or Trimethylphosphine for Ligand Addition. *J. Vac. Sci. Technol., A* **2023**, *41*, No. 032603.
(18) Partridge, J. L.; Murdzek, J. A.; Johnson, V. L.; Cavanagh, A. S.; Sharma, S.; George, S. M. Thermal Atomic Layer Etching of Gold Using Sulfuryl Chloride for Chlorination and Triethylphosphine for Ligand Addition. *Chem. Mater.* **2024**, *36*, 5149−5159.
(19) Myers, T. J.; Cano, A. M.; Lancaster, D. K.; Clancey, J. W.; George, S. M. Conversion Reactions in Atomic Layer Processing with Emphasis on ZnO Conversion to $Al_2O_3$ by Trimethylaluminum. *J. Vac. Sci. Technol., A* **2021**, *39*, No. 021001.
(20) Johnson, N. R.; George, S. M. $WO_3$ and W Thermal Atomic Layer Etching Using "Conversion-Fluorination" and "Oxidation-Conversion-Fluorination" Mechanisms. *ACS Appl. Mater. Interfaces* **2017**, *9*, 34435−34447.
(21) Cano, A. M.; Natarajan, S. K.; Partridge, J. L.; Elliott, S. D.; George, S. M. Spontaneous Etching of $B_2O_3$ by HF Gas Studied Using Infrared Spectroscopy, Mass Spectrometry, and Density Functional Theory. *J. Vac. Sci. Technol., A* **2022**, *40*, No. 022601.
(22) Cano, A. M.; Partridge, J. L.; George, S. M. Thermal Atomic Layer Etching of $Al_2O_3$ Using Sequential HF and $BCl_3$ Exposures: Evidence for Combined Ligand-Exchange and Conversion Mechanisms. *Chem. Mater.* **2022**, *34*, 6440−6449.
(23) DuMont, J. W.; Marquardt, A. E.; Cano, A. M.; George, S. M. Thermal Atomic Layer Etching of $SiO_2$ by a "Conversion-Etch" Mechanism Using Sequential Reactions of Trimethylaluminum and Hydrogen Fluoride. *ACS Appl. Mater. Interfaces* **2017**, *9*, 10296−10307.
(24) Zywotko, D. R.; George, S. M. Thermal Atomic Layer Etching of ZnO by a "Conversion-Etch" Mechanism Using Sequential Exposures of Hydrogen Fluoride and Trimethylaluminum. *Chem. Mater.* **2017**, *29*, 1183−1191.
(25) Partridge, J. L.; Abdulagatov, A. I.; Zywotko, D. R.; George, S. M. Limiting or Continuous Thermal Etching of First Row Transition Metal Oxides Using Acetylacetone and Ozone. *Chem. Mater.* **2024**, *36*, 7151−7161.
(26) Droes, S. R.; Kodas, T. T.; Hampden-Smith, M. J. Dry Etching of ZnO Films with Hexafluoroacetylacetone. *Adv. Mater.* **1998**, *10*, 1129−1133.
(27) Farkas, J.; Chi, K. M.; Hampden-Smith, M. J.; Kodas, T. T.; Dubois, L. H. Etching of Copper and Copper-Oxide at High-Rates via Generation of Volatile Copper Species. *Mater. Sci. Eng., B* **1993**, *17*, 93−96.
(28) George, M. A.; Hess, D. W.; Beck, S. E.; Ivankovits, J. C.; Bohling, D. A.; Lane, A. P. Reaction of 1,1,1,5,5,5-Hexafluoro-2,4-Pentanedione (Hhfac) with CuO, $Cu_2O$, and Cu Films. *J. Electrochem. Soc.* **1995**, *142*, 961−965.
(29) George, M. A.; Hess, D. W.; Beck, S. E.; Young, K.; Bohling, D. A.; Voloshin, G.; Lane, A. P. Reaction of 1,1,1,5,5,5-Hexafluoro-2,4-Pentanedione (Hhfac) with Iron and Iron Oxide Thin Films. *J. Electrochem. Soc.* **1996**, *143*, 3257−3266.
(30) Chen, J. K.-C.; Altieri, N. D.; Kim, T.; Chen, E.; Lill, T.; Shen, M.; Chang, J. P. Directional Etch of Magnetic and Noble Metals. II. Organic Chemical Vapor Etch. *J. Vac. Sci. Technol., A* **2017**, *35*, No. 05C305.
(31) Chen, J. K.-C.; Altieri, N. D.; Kim, T.; Lill, T.; Shen, M.; Chang, J. P. Directional Etch of Magnetic and Noble Metals. I. Role of Surface Oxidation States. *J. Vac. Sci. Technol., A* **2017**, *35*, No. 05C304.
(32) Lee, J.; Kim, J. T.; Oh, J.; Lee, D.; Lee, S. H.; Kim, H.; Oh, J.; Wang, Y.; Kim, W. H. Advanced Fabrication of Ultrathin Ruthenium Films Using Synergistic Atomic Layer Deposition and Etching. *Small Methods* **2025**, No. 202402166.
(33) Konh, M.; He, C.; Lin, X.; Guo, X. Y.; Pallem, V.; Opila, R. L.; Teplyakov, A. V.; Wang, Z. J.; Yuan, B. Molecular Mechanisms of Atomic Layer Etching of Cobalt with Sequential Exposure to Molecular Chlorine and Diketones. *J. Vac. Sci. Technol., A* **2019**, *37*, No. 021004.
(34) Konh, M.; Janotti, A.; Teplyakov, A. Molecular Mechanism of Thermal Dry Etching of Iron in a Two-Step Atomic Layer Etching Process: Chlorination Followed by Exposure to Acetylacetone. *J. Phys. Chem. C* **2021**, *125*, 7142−7154.
(35) Partridge, J. L.; Abdulagatov, A. I.; Sharma, V.; Murdzek, J. A.; Cavanagh, A.; George, S. M. Thermal Atomic Layer Etching of CoO Using Acetylacetone and Ozone: Evidence for Changes in Oxidation State and Crystal Structure during Sequential Exposures. *Appl. Surf. Sci.* **2023**, *638*, No. 157923.
(36) Mameli, A.; Verheijen, M. A.; Mackus, A. J. M.; Kessels, W. M. M.; Roozeboom, F. Isotropic Atomic Layer Etching of ZnO Using Acetylacetone and $O_2$ Plasma. *ACS Appl. Mater. Interfaces* **2018**, *10*, 38588−38595.
(37) Chittock, N. J.; Maas, J. F. W.; Tezsevin, I.; Merkx, M. J. M.; Knoops, H. C. M.; Kessels, W. M. M.; Mackus, A. J. M. Investigation of the Atomic Layer Etching Mechanism for $Al_2O_3$ Using Hexafluoroacetylacetone and $H_2$ Plasma. *J. Mater. Chem. C* **2025**, *13*, 1345−1358.
(38) Lee, J.; Oh, J.; Kim, J. T.; Oh, J.; Lee, J. M.; Kim, W. H. Atomic Layer Etching of High-k Oxide Thin Films Using Hexafluoroacetylacetone and Oxygen Radicals. *Chem. Eng. J.* **2025**, *514*, No. 163280.
(39) Hoffmann, M.; Murdzek, J. A.; George, S. M.; Slesazeck, S.; Schroeder, U.; Mikolajick, T. Atomic Layer Etching of Ferroelectric Hafnium Zirconium Oxide Thin Films Enables Giant Tunneling Electroresistance. *Appl. Phys. Lett.* **2022**, *120*, No. 122901.
(40) Murdzek, J. A.; George, S. M. Effect of Crystallinity on Thermal Atomic Layer Etching of Hafnium Oxide, Zirconium Oxide, and Hafnium Zirconium Oxide. *J. Vac. Sci. Technol., A* **2020**, *38*, No. 022608.
(41) Kim, J. Y.; Choi, M. J.; Jang, H. W. Ferroelectric Field Effect Transistors: Progress and Perspective. *APL Mater.* **2021**, *9*, No. 021102.
(42) Schroeder, U.; Park, M. H.; Mikolajick, T.; Hwang, C. S. The Fundamentals and Applications of Ferroelectric $HfO_2$. *Nat. Rev. Mater.* **2022**, *7*, 653−669.
(43) Park, J. Y.; Lee, D. H.; Park, G. H.; Lee, J.; Lee, Y.; Park, M. H. A Perspective on the Physical Scaling Down of Hafnia-Based Ferroelectrics. *Nanotechnology* **2023**, *34*, No. 202001.
(44) Kim, S. E.; Sung, J. Y.; Jeon, J. D.; Jang, S. Y.; Lee, H. M.; Moon, S. M.; Kang, J. G.; Lim, H. J.; Jung, H. S.; Lee, S. W. Toward Advanced High-k and Electrode Thin Films for DRAM Capacitors via Atomic Layer Deposition. *Adv. Mater. Technol.* **2023**, *8*, No. 2200878.
(45) Park, B. E.; Oh, I. K.; Mahata, C.; Lee, C. W.; Thompson, D.; Lee, H. B. R.; Maeng, W. J.; Kim, H. Atomic Layer Deposition of Y-

Stabilized $ZrO_2$ For Advanced DRAM Capacitors. *J. Alloys Compd.* **2017**, *722*, 307−312.
(46) Gertsch, J. C.; Sortino, E.; Bright, V. M.; George, S. M. Deposit and Etchback Approach for Ultrathin $Al_2O_3$ Films with Low Pinhole Density Using Atomic Layer Deposition and Atomic Layer Etching. *J. Vac. Sci. Technol., A* **2021**, *39*, No. 062602.
(47) Arts, K.; Utriainen, M.; Puurunen, R. L.; Kessels, W. M. M.; Knoops, H. C. M. Film Conformality and Extracted Recombination Probabilities of O Atoms during Plasma-Assisted Atomic Layer Deposition of $SiO_2$, $TiO_2$, $Al_2O_3$, and $HfO_2$. *J. Phys. Chem. C* **2019**, *123*, 27030−27035.
(48) Knoops, H. C. M.; Langereis, E.; van de Sanden, M. C. M.; Kessels, W. M. M. Conformality of Plasma-Assisted ALD: Physical Processes and Modeling. *J. Electrochem. Soc.* **2010**, *157*, G241−G249.
(49) Lee, Y.; Huffman, C.; George, S. M. Selectivity in Thermal Atomic Layer Etching Using Sequential, Self Limiting Fluorination and Ligand-Exchange Reactions. *Chem. Mater.* **2016**, *28*, 7657−7665.
(50) Partridge, J. L.; Murdzek, J. A.; Johnson, V. L.; Cavanagh, A. S.; Fischer, A.; Lill, T.; Sharma, S.; George, S. M. Thermal Atomic Layer Etching of CoO, ZnO, $Fe_2O_3$, and NiO by Chlorination and Ligand Addition Using $SO_2Cl_2$ and Tetramethylethylenediamine. *Chem. Mater.* **2023**, *35*, 2058−2068.
(51) Murdzek, J. A.; Rajashekhar, A.; Makala, R. S.; George, S. M. Thermal Atomic Layer Etching of Amorphous and Crystalline $Al_2O_3$ Films. *J. Vac. Sci. Technol., A* **2021**, *39*, No. 042602.
(52) Pinnavaia, T. J.; Fay, R. C. Preparation and Properties of Some Six- and Seven-Coordinate Halo(Acetylacetonato) Complexes of Zirconium(IV) And Hafnium(IV). *Inorg. Chem.* **1968**, *7*, 502−508.
(53) Fay, R. C.; Pinnavaia, T. J. Infrared and Raman Spectra of Some 6- 7- and 8-Coordinate Acetylacetonato Complexes of Zirconium(4) and Hafnium(4). *Inorg. Chem.* **1968**, *7*, 508−514.
(54) Mehrotra, R. C.; Bohra, R.; Gaur, D. P. *Metal Beta-Diketonates and Allied Derivatives*; Academic Press, Inc.: New York, NY, 1978.
(55) Roine, A. *HSC Chemistry 9.9.2.3*; Outokumpu Research Oy: Pori, Finland, 2019.
(56) Janiak, C.; Lange, K. C. H.; Scharmann, T. G. Zirconium-Chelate and Mons-H-Cyclopentadienyl Zirconium-Chelate/Methyl-alumoxane Systems as Soluble Ziegler-Natta Olefin Polymerization Catalysts. *Appl. Organomet. Chem.* **2000**, *14*, 316−324.
(57) Liu, Z. Y.; Jia, M.; Guo, C. Y.; He, D. W.; Hu, Y. L. Preparation of Long-Branching Polyethylene Using a Dual-Functional Catalytic System. *Acta Polym. Sin.* **2001**, 751−754.




https://doi.org/10.1021/acs.chemmater.5c01228
*Chem. Mater.* 2025, 37, 5935−5945